WARPAGE OF FLEXIBLE-BOARD ASSEMBLIES WITH BGAS DURING REFLOW AND POST-ASSEMBLY USAGE

Pradeep Lall[(1)], Kartik Goyal[(1)],
[(1)]Auburn University
NSF-CAVE3 Electronics Research Center, AL, USA
Ben Leever[(2)]
[(2)]US Air Force Research Labs, OH, USA
Jason Marsh[(3)]
[(3)]NextFlex Manufacturing Institute, CA, USA
lall@auburn.edu

ABSTRACT
Flexible printed circuit boards lack the structural stiffness of the rigid printed circuit counterparts. Thermo-mechanical deformation in flexible printed circuit assemblies may be very different from that in rigid board assemblies. The double-sided board used for the experiment is of BGA 256-144 combination with dummy components, A-PBGA256-1.0mm-17mm and A-CABGA144-1.0mm-13mm. The three-dimensional measurements of deformation and strain have been visualized on the geometry of the solder joints in the package. Digital volume correlation (DVC) method has been used to find the displacements and strains in interconnects of operational electronics. The x-ray microscopic computed tomography (μCT) system has been used to generate the 16-bit digital volume data. The x-ray detector has ability to image the x-ray attenuation of x-rays through the object. Reliability testing of SAC 305 solder interconnects has been performed on double-sided flexible circuit board using x-ray μCT by heating the package to 100℃. 3D-finite element models have been developed to ascertain the degree of error in the model prediction from non-destructive experimental measurements in reflow and thermal cycling.

INTRODUCTION
Failure in solder interconnects is one of the leading cause of reliability failure in modern electronic devices. Complexity and miniaturization of electronic assembly in today's technology trend requires these lead-free interconnects to be more robust and reliable. There are several causes which leads to an interconnect failure, such as voiding, manufacturing defects, crack, delamination, etc. If all of them are categorized, they either occur during the manufacturing stage such as during the reflow of assembly, or post-assembly usage. In addition, the type of substrate used plays an important part in determining the extent of the failure. A flexible substrate brings many advantages with it such as reducing the weight of a system as compared to rigid substrate, cost effective, heat dissipation at a better rate. On the other hand, if the substrate lacks the structural rigidity, many reliability issues may arise, such as coplanarity during manufacturing, which will further give rise to electrical failure. One of the issues, warpage, which occurs in a substrate during reflow has also been studied [1]. Substrate whether be flexible or rigid, their effect and comparison on the deformations or strains in solder interconnects must be studied. While there are numerous insightful articles on failures in solder interconnects on packages mounted on rigid printed circuit board assembly, such as detecting crack using cross-sectioning and x-ray μ-CT [2], deformations under in-situ thermal loading using optical microscope [3], creep behavior under thermal cycling using FE simulation [4], stresses and strains on plastic BGA using x-ray μ-CT with DVC [5], failure mode of SAC 305 under thermal stress [6], solder fatigue through FEA in BGA Module [7], same cannot be said for a flexible board assembly. Lack of structural rigidity in flexible circuit board assembly instigates many different aspects through which failure can occur in solder interconnects. Studies have been performed on the flexible polyimide substrate, which is generally preferred in flexible board assembly [8]-[9], due to its properties and processing capabilities such as higher T_g, high flexibility, excellent mechanical strength, thermal stability. One of the important finding from Jensen [9] is the effect of humidity on the dielectric constant of polyimide and thus electrical characteristics was under design tolerance, and how the internal stresses due to thermal expansion were below the fracture strength of polyimide. Thermo-mechanical studies are also performed for different types of packages on a flexible substrate such as BGA [10], and Ultra-Thin Chip Package [11], BGAs on flex-rigid concept substrate [12], effect of soldering on flexible substrate [13]. Not much open-literature can be found which discusses how the double-sided flexible substrate affects the solder interconnectivity under thermo-mechanical load from manufacturing aspect and post-assembly usage. In this study, thermal FE simulation is performed for the double-sided flexible assembly with BGA packages on both sides. This paper utilizes the results and data from previously published proceedings to establish a comparison between the non-destructive experimental measurements and FE simulation.

TEST VEHICLE
The test vehicle is designed to investigate the deformations and strains in solder interconnects for a BGA package mounted on a flexible circuit board accrued during reflow or post-assembly usage. The flexible circuit board consists of a

base film, polyimide, with one copper layer on both sides of it, cover film, and ENIG (Electroless Nickel Immersion Gold) surface finish.

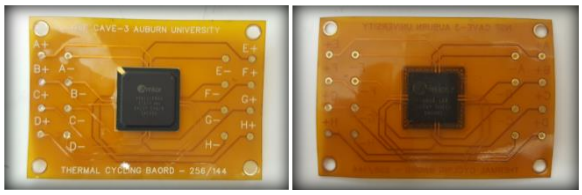

Figure 1. Flexible Printed Circuit Board

Table 1. Package Specifications

Package Type	PBGA	CABGA
I/O Count	256	144
Pitch (mm)	1.0	1.0
Ball Height (mm)	0.32	0.30
Body Size (mm)	17	13
Ball Matrix	16 x 16	12 x 12
Ball Alignment	Full-Array	Full-Array
Solder Ball Material	Sn3Ag0.5Cu	Sn3Ag0.5Cu

The circuit board is of 2.5″ × 1.7″ with a total thickness of 0.15mm. The assembly consists of double-sided flexible board with PBGA 256 on one side and CABGA 144 on the other as shown in Figure 1. Both packages have pitch of 1mm. Table 1 shows the package specifications. SAC 305 lead-free alloy is used for the solder joint material, and Anand model was implemented as the constitutive model to describe the material behavior. Table 2 below lists the Anand parameters for SAC 305 used in this study [14].

Table 2. Anand Parameters for SAC 305 [14]

Anand Constant	*Units*	*SAC 305*
s_o	MPa	21.0
Q/R	1/K	9320
A	sec^{-1}	3501
ξ	-	4
M	-	0.25
h_o	MPa	180000
$\hat{s}$	MPa	30.2
n	-	0.01
a	-	1.78

FINITE ELEMENT MODEL

In this article, ANSYS Mechanical APDL is used to develop quarter model due to symmetry of both, flexible and rigid assembly. To produce good results in any simulation, it is required to have the dimensions correctly. To have that, the assembly was cross-sectioned and optical microscopy was used to measure the thickness of each layer in flexible board and rigid board. All the dimensions and material properties are listed in Table 3 [14]-[15]. All the solid layers are modeled using SOLID45 element, whereas the solder joint is modeled as VISCO107. According to the design of assembly, the backside of the model, which is CABGA 144, is set to be at an offset of 0.1mm. Because of that offset, MPC algorithm was used to glue the uneven mesh created on the printed circuit board. The quarter model of one solder joint on a flexible board with the offset is shown in Figure 2 and Figure 3. The quarter model for the flexible assembly is meshed with hexahedra elements.

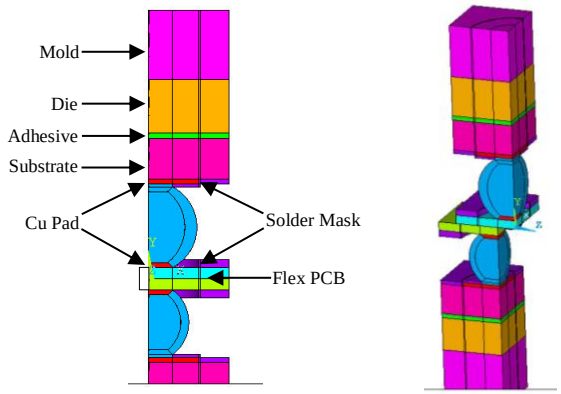

Figure 2. Quarter Model of Solder Joint on Flexible Assembly

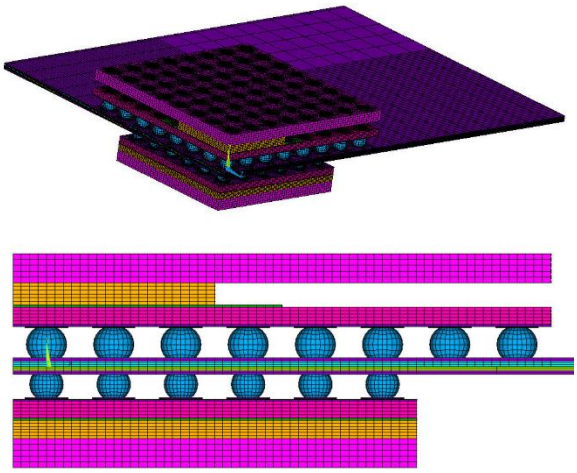

Figure 3. Meshed Quarter Model Flexible Printed Circuit Board

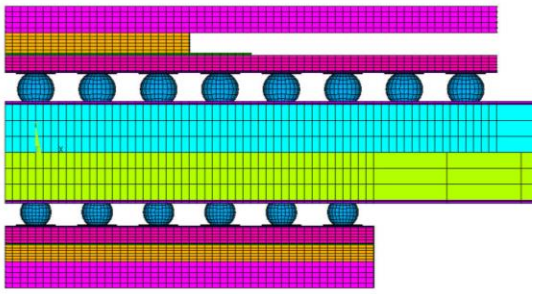

Figure 4. (top and bottom) Meshed Quarter Model Rigid Printed Circuit Board

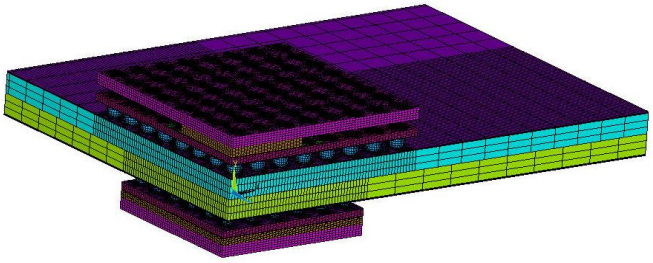

Figure 5. Meshed Quarter Model Rigid Printed Circuit Board

Table 3. Material Properties

	Thickness (mm)		Elastic Modulus (MPa)		Shear Modulus (MPa)		Poisson's Ratio		Coefficient of Thermal Expansion (ppm/°C)	
Printed Circuit Board	*Flexible Substrate* [15]	0.14	2,500		-		0.34		20	
	Rigid Substrate	1.55	E_x	17,000	G_{xy}	3,324	v_{xy}	0.39	α_x	14.5
			E_y	7,436	G_{yz}	3,324	v_{yz}	0.39	α_y	67.2
			E_z	17,000	G_{xz}	7,623	v_{xz}	0.11	α_z	14.5
Solder Mask	0.05		3,100		-		0.3		30	
Cu Pad	0.03		128,932		-		0.34		16.3	
Solder Ball	*PBGA 256*	0.5(height); 0.64 (dia)	54,000		-		0.35		24	
	CABGA 144	0.4 (height); 0.5 (dia)								
Substrate	0.25		E_x	17,890	G_{xy}	2,822	v_{xy}	0.39	α_x	12.4
			E_y	7,846	G_{yz}	2,822	v_{yz}	0.39	α_y	57
			E_z	17,890	G_{xz}	8,061	v_{xz}	0.11	α_z	12.4
Adhesive	0.035		6,769		-		0.35		52	
Die	*PBGA 256*	0.33	162,716		-		0.28		2.54	
	CABGA 144	0.27								
Mold	0.43		23,520		-		0.3		15	

Similarly, model was developed and meshed with hexahedra elements for rigid assembly and is shown in Figure 4,

.

FE LOADS AND BOUNDARY CONDITION

The loading applied to the FE model is a thermal load of 100°C to replicate it with the experimental measurements done previously. Initially, the package was assumed to be at room temperature 23°C, stress-free state with no residual stresses which may have induced during the manufacturing process. Additionally, it is assumed that the whole assembly is subjected to 100°C, i.e. there is no loss of heat in the assembly between mold and the printed circuit board. Symmetry was enforced, and the model was appropriately constrained along the axis of symmetry so that the normal displacement component acting at a node on the symmetry plane was zero. To prevent any rigid body motion, all three-displacement components were set to be zero for the bottom-most node in the quarter model. For the uneven mesh obtained due to the offset of the bottom package, Multi-Point Constraint (MPC) approach is used. MPC technique is used to establish a contact relation between two areas or volumes to prevent penetration using extra pair of elements defined between them. In this study, surface-to-surface contact model at the neutral axis of PCB is used to establish the MPC relations and eliminate the DOF's to glue the two halves and the mesh elements.

EXPERIMENTAL TEST SETUP

The effect of thermal load of 100°C on the SAC 305 solder interconnects on the double-sided flexible printed circuit board is presented. The x-ray system is similar to an industrial computed tomography scanner, which offers very high-resolution volume slices, which are rendered together in 3D to provide a full 3D volume and can be used to analyze internal details or on a slice-by-slice basis at a user specified location.

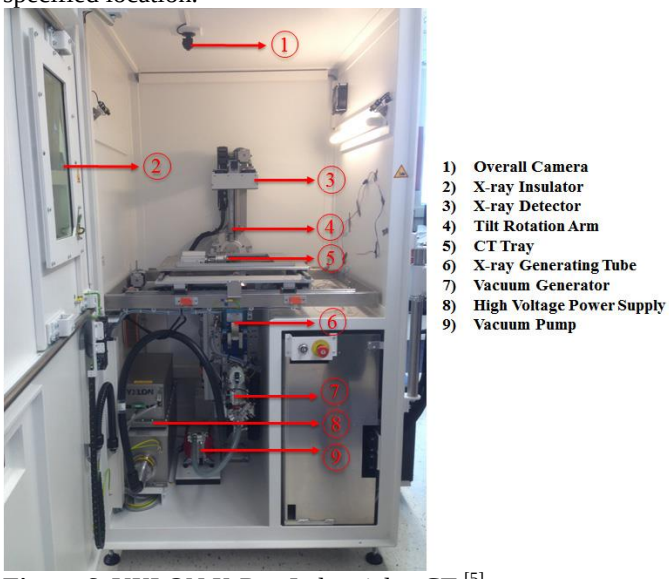

Figure 6. YXLON X-Ray Industrial µ-CT [5]

The process of analyzing the package in µ-CT involves 360° rotation of the package while in the field of x-ray beam and capturing the volume slices at different angles while rotating. This process was repeated for two states of the region of interest: undeformed and deformed, and the region of interest being the die-shadow. The YXLON µ-CT Cougar Machine used for the experiment shown in Figure 6, is a state-of-art machine with detail detectability of < 1µm**Error! Reference source not found.**. The full scan system is shown in Figure 7, which includes the µ-CT CPU and the reconstruction CPU. The necessary acceleration voltage was provided to direct the electron beam and the

necessary current, which heats up the tungsten filament to determine the power to the beam. Parts tested in the system have no adverse effect from the exposure to the beam, which makes it possible to run multiple scans. The 3D rendered volume is then exported as standard DICOM slices, which are the input to DVC. Digital volume correlation (DVC), an extended version of digital image correlation (DIC), is a non-destructive technique to measure the 3D deformation or strain field present internally and on the surface of the object. DVC tracks voxels in two sets of images as compared to pixels in DIC. To obtain the deformation or strain field, the DICOM slices obtained from the µ-CT are re-constructed to form a 3D matrix of grayscale values, in which each layer represents a cross-section plane with grayscale value at every voxel in that plane. Higher density material, such as solder joint will have a higher grayscale value and lower density material such as the fixture made of ABS plastic material will have a lower value. With multiple trials, a threshold value was set to focus the DVC algorithm on the die-shadow solder balls only and ignore the rest for the sake of decreasing computation time. Figure 8 shows the die-shadow solder balls volume for the flexible board obtained for the pre-visualization. This is the input volume or matrix used to perform correlation analysis to calculate deformation and strains. The deformation field is obtained by correlating the grayscale values in the two states of volume. The strain field is calculated from the gradients of the deformation.

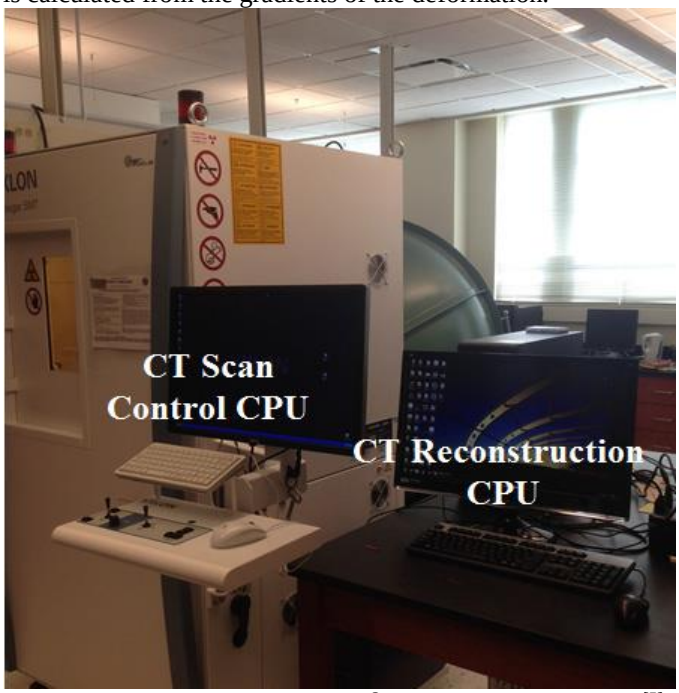

Figure 7. X-Ray µ-CT at CAVE^3 Auburn University, AL [5]

Similar to digital image correlation, the accuracy of the results depend on 3D subset size or a voxel size, which should be big enough to contain distinct grayscale values; region of interest in which the search algorithm should be performed to find the respective voxel in the deformed state. The voxel subset is a cubic window of the volume, center of which is the start point of the computation. This start point is used to compute the correlation coefficient between the voxel windows in undeformed and in deformed. To find the best matching voxel window in deformed state, a search algorithm is performed which steps up in x, y, and z-direction until a best match is found in 3D space. The best correlation will provide the biggest correlation coefficient. The algorithm used to calculate deformation is normalized cross-correlation function, Equation (1) which is based on minimizing the correlation coefficients.

$$C = 1 - \frac{\sum_{i=1}^{L}\sum_{j=1}^{M}\sum_{k=1}^{N}\left(V_{ijk} - \overline{V}\right)\left(V'_{ijk} - \overline{V}'\right)}{\sqrt{\sum_{i=1}^{L}\sum_{j=1}^{M}\sum_{k=1}^{N}\left(V_{ijk} - \overline{V}\right)^2\left(V'_{ijk} - \overline{V}'\right)^2}} \quad (1)$$

where, C is the quantity or an error from the correlation, V contains the grayscale values of the voxels, and $\overline{V}$ contains the mean of the grayscale values present in the subset being examined. The maximum error in the algorithm is one when the algorithm is not able to find the defined voxel window and the minimum is zero when the algorithm can find the exact voxel window in the deformed state.

DEFORMATION AND STRAIN MEASUREMENT

In this section, deformation and strain measurements in the die-shadow solder joints are presented. These measurements are performed on the die-shadow area of PBGA 256 only when 100°C thermal load was applied on it. The DVC deformation and strain measurements are plotted on the original or reference volume. DVC was performed on the flexible circuit board initially, and then on the rigid circuit board of the same configuration to compare the deformation and strain. The deformation and strains in x and z-direction represents the in-plane coordinate system, while the y-direction represents the out of plane coordinate.

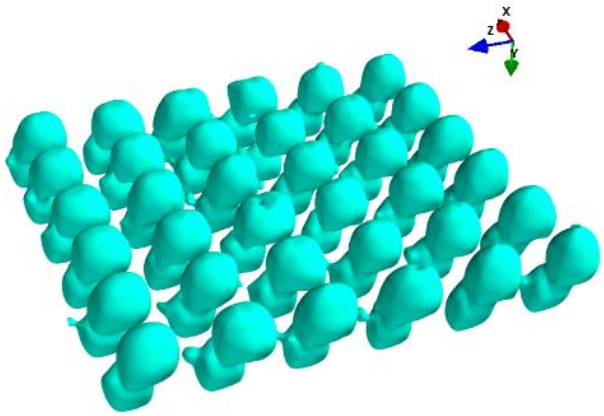

Flexible Circuit Board (Thermal Load on PBGA 256)

The deformation and strain field in die-shadow solder joints on the flexible circuit board is presented. Due to very small thickness of the flexible substrate (polyimide), the CABGA

144 solder balls under PBGA 256 were also considered in the computation. This way, the effect of applying thermal load on PBGA 256 can also be analyzed in CABGA 144. The deformation in x, y, and z-direction can be seen in Figure 9 to Figure 11. From the contours, we can see that the solder joints experienced most of the deformation in y-direction, the direction in which thermal load was applied, with maximum area of solder joint having maximum of 0.11 mm. Maximum variations in the contours are also seen in y-direction as compared to x and z-deformation. In the x-direction, the deformation field is significantly different relative to y and z-direction, having values in the range of ±0.08 mm. In the z-direction, some part of the solder joint does experience maximum deformation of 0.11 mm, but most of the area experienced values in the range of ±0.05 mm.

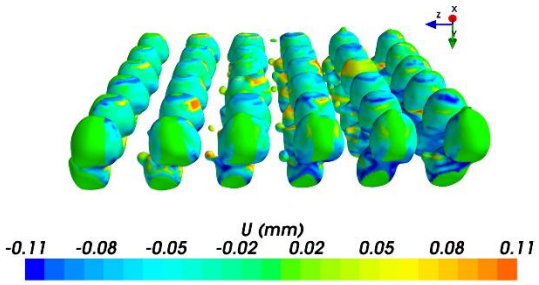

Figure 9. Deformation in X-Direction

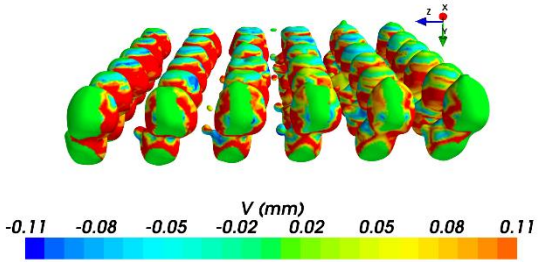

Figure 10. Deformation in Y-Direction

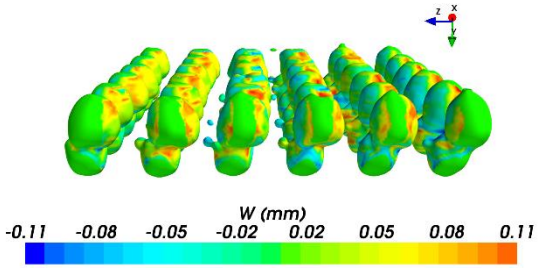

Figure 11. Deformation in Z-Direction

Shear strains are also plotted as shown in Figure 12 to Figure 14. From the measurements, it can be seen the shear strain in y-z direction is very large as compared to strains in x-y and x-z direction. Strains in x-y direction experience most of the values in the range of ±0.13 µ-strains while strains in x-z has values in the neighborhood of -0.05 µ-strains. In the case of strains in y-z direction, most of the solder joints experience strains in the range of ±0.50 mm with a maximum of 1.63 µ-strain the positive z-direction and 2.10 µ-strains in the negative z-direction.

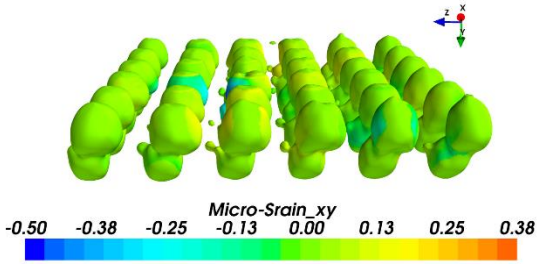

Figure 12. Strain in x-y Direction

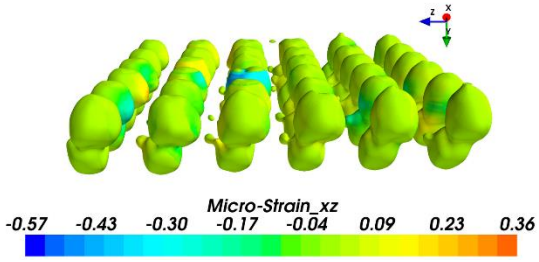

Figure 13. Strain in x-z Direction

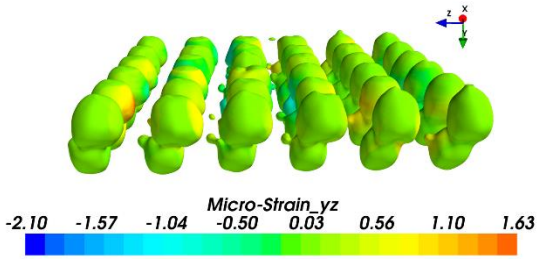

Figure 14. Strain in y-z Direction

Rigid Circuit Board (Thermal Load on PBGA 256)

Deformations and strains are measured in the PBGA 256 die-shadow solder joints on a rigid printed circuit board when subjected to thermal load of 100°C. In the case of rigid circuit board, the FR-4 substrate thickness is very large as compared to the polyimide in flexible, due to which only PBGA 256 die-shadow solder balls were considered for the sake of reducing the computation time. Figure 15 shows the pre-visualized input volume used to perform correlation between reference and deformed state. Deformations rendered on the reference volume in x, y, and z-direction are shown in Figure 16 to Figure 18. From the contours, it can be seen that there is not much discontinuity in the deformation field as compared to the flexible circuit board. In the case of x-direction, most of the solder joints

experience the deformation around the magnitude of about ~0.01 mm. In y-direction, the magnitude of deformation is same as x-direction, but in the positive direction, which should be because of the thermal load applied in positive y-direction. Not much variation in the deformation field is seen in the case of z-direction deformation.

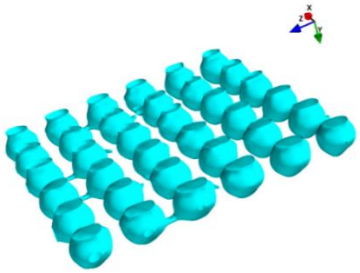

Figure 15. Pre-Visualization of PBGA 256 Die-Shadow for Rigid Board

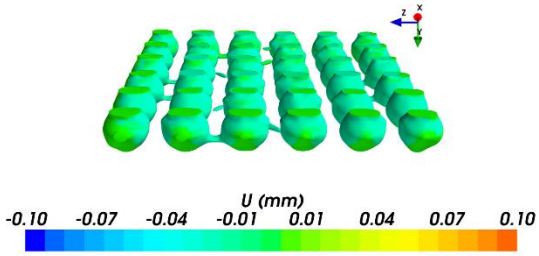

Figure 16. Deformation in X-Direction

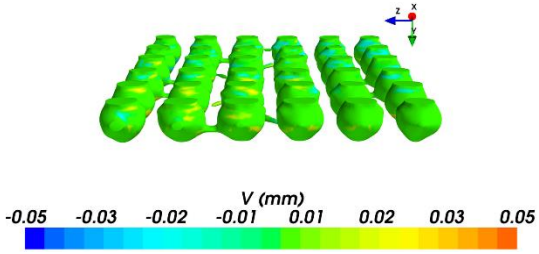

Figure 17. Deformation in Y-Direction

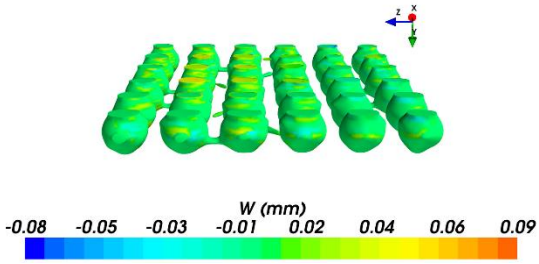

Figure 18. Deformation in Z-Direction

Shear strains were also plotted shown in Figure 19 to Figure 21. Strains in x-y direction are the lowest as compared to x-z and y-z direction, with a maximum of 0.06 µ-strains. The highest strains are seen in x-z direction with maximum of 0.22 µ-strains. Strain field in y-z direction is very continuous as compared to the other two and fall in the neighborhood of 0.03 µ-strains.

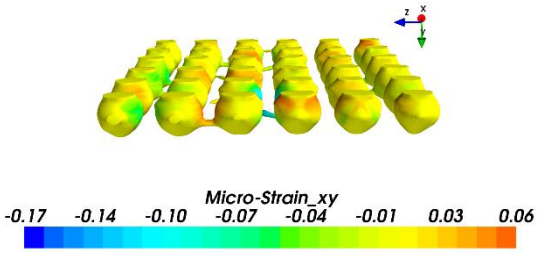

Figure 19 Strain in x-y Direction

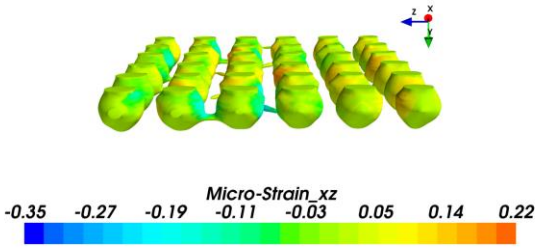

Figure 20 Strain in x-z Direction

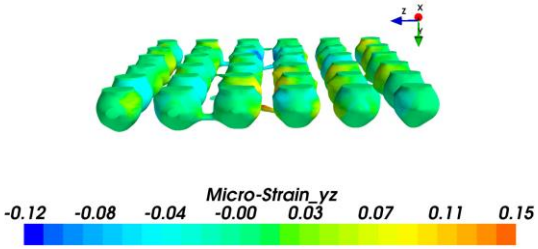

Figure 21 Strain in y-z Direction

FEA RESULTS AND DISCUSSION

Reliability of solder joint in an electronic package has been measured by the plastic work energy, which is accumulated by the external load imposed on it. In our study, the external load is the thermal temperature of 100°C applied on the package, which induces plastic work due to coefficient of thermal expansion (CTE) mismatch between different materials in an assembly. In addition, shear strains are also used to study reliability to determine if there is any delamination, crack, or void which may have occurred during the thermo-mechanical load.

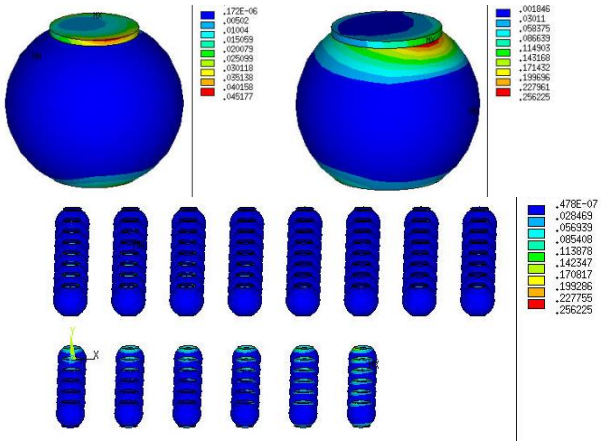

Figure 22. Plastic Work per unit Volume for Rigid Assembly. (top left) Corner Joint for Top Package. (top right) Corner Joint for Bottom Package. (bottom) Quarter Model.

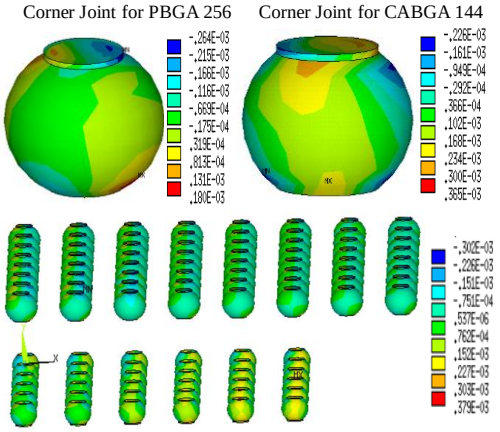

Figure 23. Strain Component in x-y for Rigid Assembly. (top left) Corner Joint for Top Package. (top right) Corner Joint for Bottom Package. (bottom) Quarter Model.

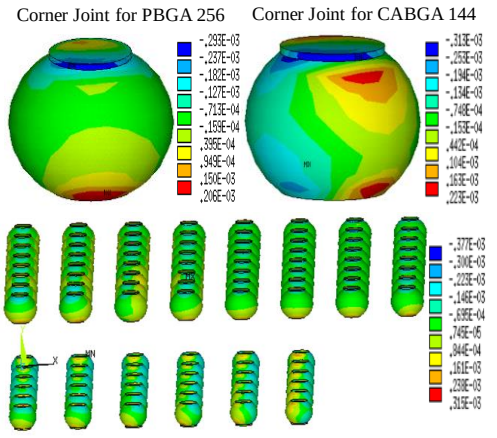

Figure 24 Strain component in y-z for Rigid Assembly. (top left) Corner Joint for Top Package. (top right) Corner Joint for Bottom Package. (bottom) Quarter Model.

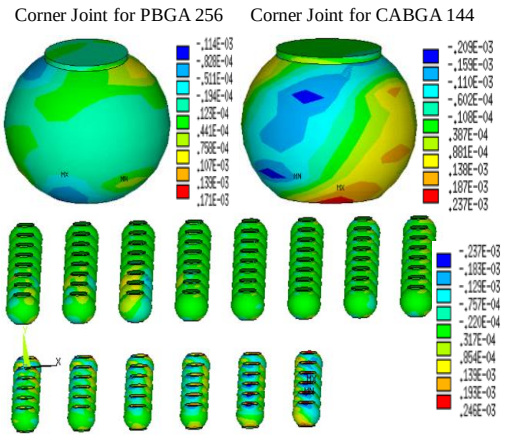

Figure 25. Strain component in x-z for Rigid Assembly. (top left) Corner Joint for Top Package. (top right) Corner Joint for Bottom Package. (bottom) Quarter Model.

In this manuscript, contours of both, plastic work energy per unit volume and shear strains are plotted and are enlarged for the corner joints of top and bottom package. These strains are then compared with the previously published experimental measurements obtained non-destructively using DVC. Figure 22 shows the plastic work energy per unit volume of the solder joints on a rigid assembly which shows maximum of 0.25 MPa at the corner joint for the bottom package, while for the top package, it is about 0.04 MPa.

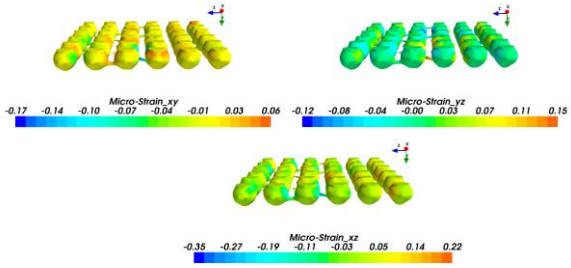

Figure 26. Previously Established Digital Volume Correlation Strain Results for Rigid Board

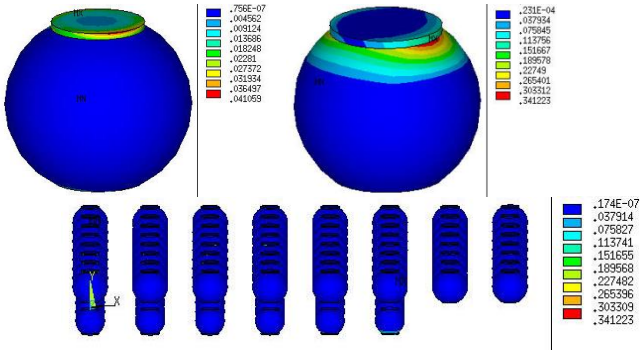

Figure 27. Plastic Work per unit Volume for Flexible Assembly. (top left) Corner Joint for Top Package. (top right) Corner Joint for Bottom Package. (bottom) Quarter Model.

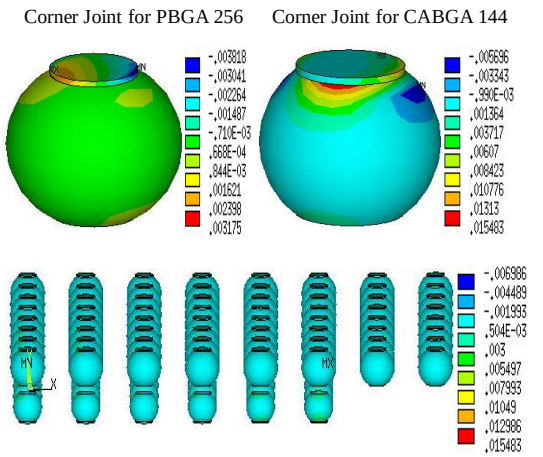

Figure 28. Strain Component in x-y for Flexible Assembly. (top left) Corner Joint for Top Package. (top right) Corner Joint for Bottom Package. (bottom) Quarter Model.

In both packages, the maximum energy is seen at the interface of solder joint and copper pad towards the package side, which would result in delamination. Figure 23, Figure 24, Figure 25shows the contours for shear strains in x-y, y-z, and x-z direction respectively. Strain in the x-y direction is maximum at the interface of copper pad towards the substrate and bottom solder joint. Strain in y-z and x-z direction is about 0.05 µ-Strains. These strain findings for rigid assembly are well enough in range with the experimental values from non-destructive method, DVC. Previously, for the rigid assembly, only the solder joints under the die shadow of PBGA 256 were considered. Figure 26 shows the previously established DVC results. Similarly, contours of plastic work energy per unit volume and shear strains for flexible assembly are plotted. Figure 27 shows the plastic work energy per unit volume is maximum at the corner joint for the bottom package, which is about 0.34 MPa, little higher as compared to rigid assembly, and 0.04 MPa at the joint for the top package, which is same as in case of rigid assembly.

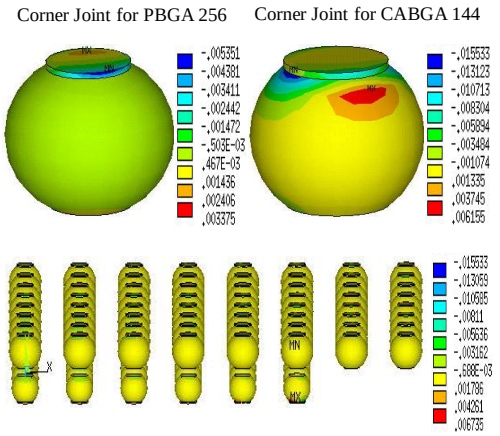

Figure 29. Strain Component in y-z for Flexible Assembly. (top left) Corner Joint for Top Package. (top right) Corner Joint for Bottom Package. (bottom) Quarter Model.

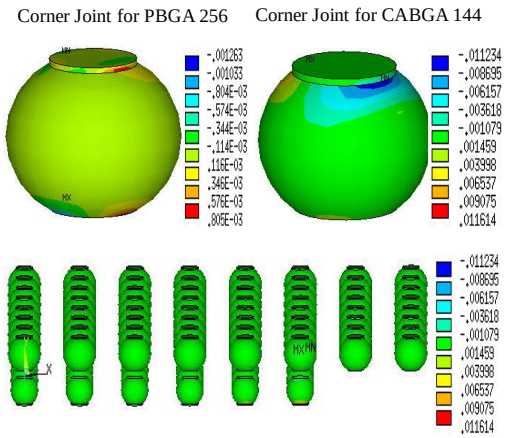

Figure 30. Strain Component in x-z for Flexible Assembly. (top left) Corner Joint for Top Package. (top right) Corner Joint for Bottom Package. (bottom) Quarter Model.

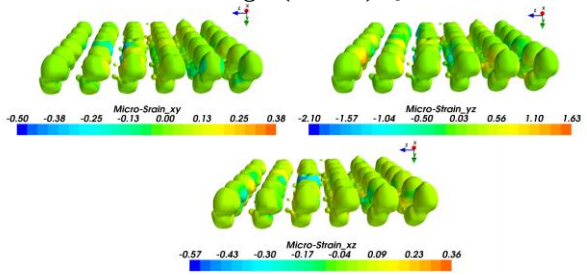

Figure 31. Previously Established Digital Volume Correlation Strain Results for Flexible Board

Figure 28, Figure 29, Figure 30 shows the contours for shear strains. The location for maximum strain in x-y and x-z appears to be at the interface of copper pad and solder joint for the bottom package. Strain in y-z is maximum at somewhere middle of bottom corner joint, which can be argued as the location where crack initiates. The strain findings for flexible assembly also agree with the experimental measurements using DVC. Previously, for flexible assembly, due to the substrate thickness, solder joints under the die shadow of PBGA 256 for both, top and bottom package were considered and evaluated. Figure 31 shows the previously established DVC strain results.

Table 4. Comparison of Strains from DVC and FE Simulation

	Rigid		Flexible	
µ-Strains	*DVC*	*FE*	*DVC*	*FE*
x-y Strain	~ [0.01-0.06]	~ 0.07	~ [0-0.13]	~ 0.07
y-z Strain	~ [0.03-0.07]	~ 0.07	~ [0.03-0.56]	~ 0.50
x-z Strain	~ [0.03-0.05]	~ 0.03	~ [0.04-0.09]	~ 0.10

SUMMARY AND CONCLUSIONS

In this study, non-destructive DVC have been used to measure the thermo-mechanical deformation of solder joints in flexible and rigid printed circuit assemblies. Measurements from DVC have been compared with FE

model predictions to determine the error in strain measurements. The quarter-model is developed for a double-sided assembly with flexible and rigid substrate, to simulate the non-linear thermo-mechanical damage in solder joints using the Anand constitutive model. The MPC approach is also utilized in this paper to glue the uneven mesh obtained due to the offset of the bottom package. This study has been performed on a double-sided test assembly, which consists of BGA packages on two different substrates: rigid and flexible. The top package, PBGA 256 was subjected to thermal load of 100°C, and the effect of it is measured on both, top and bottom package. Both daisy-chain BGA components have pitch of 1mm. For FE simulation, symmetry was enforced, and appropriate boundary conditions were applied. The findings from FE analysis and experimental DVC correlate well with each other as shown in Table 4 above, which establishes DVC, when used in conjunction with x-ray µ-CT as a very reliable technique to determine the deformations or strains and visualize them as they are on the object itself without physically destroying it.

ACKNOWLEDGEMENTS

The project was sponsored by the NextFlex Manufacturing Institute under PC 2.5 Project titled – Mechanical Test Methods for Flexible Hybrid Electronics Materials and Devices.

REFERENCES

[1] P. Lall and K. Goyal, "Study on the effect of fixtures on deformation and warpage of the double-sided flexible printed circuit board through reflow using DIC," *2017 16th IEEE Intersociety Conference on Thermal and Thermomechanical Phenomena in Electronic Systems (ITherm)*, Orlando, FL, 2017, pp. 1306-1314.

[2] P. Lall, S. Deshpande, J. Wei and J. Suhling, "Non-destructive crack and defect detection in SAC solder interconnects using cross-sectioning and X-ray micro-CT," *2014 IEEE 64th Electronic Components and Technology Conference (ECTC)*, Orlando, FL, 2014, pp. 1449-1456.

[3] Seungbae Park, Ramji Dhakal, Lawrence Lehman, Eric Cotts, Measurement of deformations in SnAgCu solder interconnects under in situ thermal loading, Acta Materialia, Volume 55, Issue 9, May 2007, Pages 3253-3260, ISSN 1359-6454.

[4] X. Li, L. Wang and H. Liu, "Simulation study on creep behavior of BGA solder joints under temperature cycling," *2016 17th International Conference on Electronic Packaging Technology (ICEPT)*, Wuhan, 2016, pp. 669-673.

[5] P. Lall and J. Wei, "PBGA package Finite Element Analysis based on the physical geometry modeling using X-ray micro CT digital volume reconstruction," *2016 15th IEEE Intersociety Conference on Thermal and Thermomechanical Phenomena in Electronic Systems (ITherm)*, Las Vegas, NV, 2016, pp. 285-294.

[6] C. Huang, D. Yang, B. Wu, L. Liang and Y. Yang, "Failure mode of SAC305 lead-free solder joint under thermal stress," *2012 13th International Conference on Electronic Packaging Technology & High Density Packaging*, Guilin, 2012, pp. 1395-1398.

[7] J. Zhang, Q. Ji and L. Rector, "Solder Fatigue Study through Finite Element Analysis in a Molded Board Level BGA Module," *2007 International Symposium on High Density packaging and Microsystem Integration*, Shanghai, 2007, pp. 1-6.

[8] Ying-Chih Wu, Yu-Jung Huang, Ming-Kun Chen, Yi-Lung Lin and Shen-Li Fu, "Failure analysis of Cu electroplating process with Polyimide substrate fabricated for flexible packaging," *2012 7th International Microsystems, Packaging, Assembly and Circuits Technology Conference (IMPACT)*, Taipei, 2012, pp. 94-97.

[9] R. Jensen, J. Cummings and H. Vora, "Copper/polyimide Materials System for High Performance Packaging," in *IEEE Transactions on Components, Hybrids, and Manufacturing Technology*, vol. 7, no. 4, pp. 384-393, Dec 1984.

[10] F. Hou et al., "Thermo-mechanical reliability study for 3D package module based on flexible substrate," 2013 14th International Conference on Electronic Packaging Technology, Dalian, 2013, pp. 1296-1300.

[11] M. Gonzalez et al., "Thermo-mechanical analysis of flexible and stretchable systems," 2010 11th International Thermal, Mechanical & Multi-Physics Simulation, and Experiments in Microelectronics and Microsystems (EuroSimE), Bordeaux, 2010, pp. 1-7.

[12] L. Arruda, Q. Chen and J. Quintero, "Failure evaluation of flexible-rigid PCBs by thermo-mechanical simulation," 2009 International Conference on Electronic Packaging Technology & High Density Packaging, Beijing, 2009, pp. 1201-1205.

[13] M. J. Rizvi, C. Y. Yin and C. Bailey, "Modeling the Effect of Lead-free Soldering on Flexible Substrates," 2006 International Conference on Electronic Materials and Packaging, Kowloon, 2006, pp. 1-5

[14] M. M. Basit *et al*., "Thermal cycling reliability of aged PBGA assemblies - comparison of Weibull failure data and finite element model predictions," *2015 IEEE 65th Electronic Components and Technology Conference (ECTC)*, San Diego, CA, 2015, pp. 106-117.

[15] http://www.dupont.com/content/dam/dupont/products-and-services/membranes-and-films/polyimde-films/documents/DEC-Kapton-summary-of-properties.pdf.

[16] Lall P, Goyal K. Reliability of SAC 305 Solder Interconnects on Double-Sided Flexible Printed Circuit Board Using X-Ray Micro-CT. ASME. International Electronic Packaging Technical Conference and Exhibition, *ASME 2017 International Technical Conference and Exhibition on Packaging and Integration of Electronic and Photonic Microsystems.*